

Electron beam lithography designed silver nano-disks used as label free nano-biosensors based on localized surface plasmon resonance

Neval A. Cinel,^{1,2,*} Serkan Bütün,^{1,3} and Ekmel Özbay^{1,2,3}

¹Nanotechnology Research Center, Bilkent University, 06800 Bilkent, Turkey

²Department of Electrical and Electronics Engineering, Bilkent University, 06800 Bilkent, Turkey

³Department of Physics, Bilkent University, 06800 Bilkent, Turkey

*nyilmaz@ee.bilkent.edu.tr

Abstract: We present a label-free, optical nano-biosensor based on the Localized Surface Plasmon Resonance (LSPR) that is observed at the metal-dielectric interface of silver nano-disk arrays located periodically on a sapphire substrate by Electron-Beam Lithography (EBL). The nano-disk array was designed by finite-difference and time-domain (FDTD) algorithm-based simulations. Refractive index sensitivity was calculated experimentally as 221-354 nm/RIU for different sized arrays. The sensing mechanism was first tested with a biotin-avidin pair, and then a preliminary trial for sensing heat-killed Escherichia coli (E. coli) O157:H7 bacteria was done. Although the study is at an early stage, the results indicate that such a plasmonic structure can be applied to bio-sensing applications and then extended to the detection of specific bacteria species as a fast and low cost alternative.

©2012 Optical Society of America

OCIS codes: (170.0170) Medical optics and biotechnology; (220.4241) Nanostructure fabrication; (280.1415) Biological sensing and sensors; (240.6680) Surface plasmons

References and links

1. Anonymous, "ISO 9308-1," (ISO, Geneva, Switzerland, 2000).
2. P. Daly, T. Collier, and S. Doyle, "PCR-ELISA detection of Escherichia coli in milk," *Letts. Appl. Microbiol.* **34**(3), 222–226 (2002).
3. B. L. Dylla, E. A. Vetter, J. G. Hughes, and F. R. Cockerill 3rd, "Evaluation of an immunoassay for direct detection of Escherichia coli O157 in stool specimens," *J. Clin. Microbiol.* **33**(1), 222–224 (1995).
4. R. P. Johnson, R. J. Durham, S. T. Johnson, L. A. MacDonald, S. R. Jeffrey, and B. T. Butman, "Detection of Escherichia coli O157:H7 in meat by an enzyme-linked immunosorbent assay, EHEC-Tek," *Appl. Environ. Microbiol.* **61**(1), 386–388 (1995).
5. M. A. Cooper, "Optical biosensors in drug discovery," *Nat. Rev. Drug Discov.* **1**(7), 515–528 (2002).
6. J. Homola, S. S. Yee, and G. Gauglitz, "Surface plasmon resonance sensors: review," *Sens. Actuators B Chem.* **54**(1-2), 3–15 (1999).
7. X. Y. Liu, X. D. Zeng, N. N. Mai, Y. Liu, B. Kong, Y. H. Li, W. Z. Wei, and S. L. Luo, "Amperometric glucose biosensor with remarkable acid stability based on glucose oxidase entrapped in colloidal gold-modified carbon ionic liquid electrode," *Biosens. Bioelectron.* **25**(12), 2675–2679 (2010).
8. I. Vostiar, J. Tkac, E. Sturdik, and P. Gemeiner, "Amperometric urea biosensor based on urease and electropolymerized toluidine blue dye as a pH-sensitive redox probe," *Bioelectrochemistry* **56**(1-2), 113–115 (2002).
9. A. Malave, M. Tewes, T. Gronewold, and M. Lohndorf, "Development of impedance biosensors with nanometer gaps for marker-free analytical measurements," *Microelectron. Eng.* **78–79**, 587–592 (2005).
10. W. Zhao, J. J. Xu, and H. Y. Chen, "Electrochemical biosensors based on layer-by-layer assemblies," *Electroanalysis* **18**(18), 1737–1748 (2006).
11. M. H. Meyer, M. Stehr, S. Bhuju, H. J. Krause, M. Hartmann, P. Miethe, M. Singh, and M. Keusgen, "Magnetic biosensor for the detection of Yersinia pestis," *J. Microbiol. Methods* **68**(2), 218–224 (2007).
12. J. Llandro, J. J. Palfreyman, A. Ionescu and C. H. Barnes, "Magnetic biosensor technologies for medical applications: a review," *Med. Biol. Eng. Comput.* **48**(10), 977–998 (2010).
13. X. Fan, I. M. White, S. I. Shopova, H. Zhu, J. D. Suter, and Y. Sun, "Sensitive optical biosensors for unlabeled targets: a review," *Anal. Chim. Acta* **620**(1-2), 8–26 (2008).
14. K. E. Shafer-Peltier, C. L. Haynes, M. R. Glucksberg, and R. P. Van Duyne, "Toward a glucose biosensor based on surface-enhanced Raman scattering," *J. Am. Chem. Soc.* **125**(2), 588–593 (2003).

15. M. Kahraman, M. M. Yazici, F. Sahin, O. F. Bayrak, and M. Culha, "Reproducible surface-enhanced Raman scattering spectra of bacteria on aggregated silver nanoparticles," *Appl. Spectrosc.* **61**(5), 479–485 (2007).
16. F. S. Ligler and C. A. R. Taitt, *Optical Biosensors: Present and Future*, 1st ed. (Elsevier, 2002), pp. viii, 607 p.
17. L. S. Jung, C. T. Campbell, T. M. Chinowsky, M. N. Mar, and S. S. Yee, "Quantitative interpretation of the response of surface plasmon resonance sensors to adsorbed films," *Langmuir* **14**(19), 5636–5648 (1998).
18. A. J. Haes and R. P. Van Duyne, "A unified view of propagating and localized surface plasmon resonance biosensors," *Anal. Bioanal. Chem.* **379**(7-8), 920–930 (2004).
19. M. D. Malinsky, K. L. Kelly, G. C. Schatz, and R. P. Van Duyne, "Chain length dependence and sensing capabilities of the localized surface plasmon resonance of silver nanoparticles chemically modified with alkanethiol self-assembled monolayers," *J. Am. Chem. Soc.* **123**(7), 1471–1482 (2001).
20. J. C. Riboh, A. J. Haes, A. D. McFarland, C. Ranjit Yonzon, and R. P. Van Duyne, "A nanoscale optical biosensor: Real-time immunoassay in physiological buffer enabled by improved nanoparticle adhesion," *J. Phys. Chem. B* **107**(8), 1772–1780 (2003).
21. Z. T. Liu, M. D. Thoreson, A. V. Kildishev, and V. M. Shalaev, "Translation of nanoantenna hot spots by a metal-dielectric composite superlens," *Appl. Phys. Lett.* **95**, 033114 (2009).
22. Z. Liu, A. Boltasseva, R. H. Pedersen, R. M. Bakker, A. V. Kildishev, V. P. Drachev, and V. M. Shalaev, "Plasmonic nanoantenna arrays for the visible," *Metamaterials (Amst.)* **2**(1), 45–51 (2008).
23. E. Hutter and J. H. Fendler, "Exploitation of localized surface plasmon resonance," *Adv. Mater. (Deerfield Beach Fla.)* **16**(19), 1685–1706 (2004).
24. J. Zhao, X. Zhang, C. R. Yonzon, A. J. Haes, and R. P. Van Duyne, "Localized surface plasmon resonance biosensors," *Nanomedicine (Lond)* **1**(2), 219–228 (2006).
25. K. A. Willets and R. P. Van Duyne, "Localized surface plasmon resonance spectroscopy and sensing," *Annu. Rev. Phys. Chem.* **58**(1), 267–297 (2007).
26. J. N. Anker, W. P. Hall, O. Lyandres, N. C. Shah, J. Zhao, and R. P. Van Duyne, "Biosensing with plasmonic nanosensors," *Nat. Mater.* **7**(6), 442–453 (2008).
27. F. Y. Lee, K. H. Fung, T. L. Tang, W. Y. Tam, and C. T. Chan, "Fabrication of gold nano-particle arrays using two-dimensional templates from holographic lithography," *Curr. Appl. Phys.* **9**(4), 820–825 (2009).
28. A. Hohenau, H. Ditlbacher, B. Lamprecht, J. R. Krenn, A. Leitner, and F. R. Aussenegg, "Electron beam lithography, a helpful tool for nanooptics," *Microelectron. Eng.* **83**(4-9), 1464–1467 (2006).
29. C. Vieu, F. Carcenac, A. Pepin, Y. Chen, M. Mejias, A. Lebib, L. Manin-Ferlazzo, L. Couraud, and H. Launois, "Electron beam lithography: resolution limits and applications," *Appl. Surf. Sci.* **164**(1-4), 111–117 (2000).
30. A. A. Tseng, K. Chen, C. D. Chen, and K. J. Ma, "Electron beam lithography in nanoscale fabrication: recent development," *IEEE Trans. Electron. Packag. Manuf.* **26**(2), 141–149 (2003).
31. P. Rai-Choudhury, *Handbook of Microlithography, Micromachining, and Microfabrication*, IEE materials and devices series (SPIE Optical Engineering Press, 1997).
32. Pierce, *Avidin-Biotin Technical Handbook* (Thermo Scientific, 2010).
33. J. X. Fu, A. Collins, and Y. P. Zhao, "Optical properties and biosensor application of ultrathin silver films prepared by oblique angle deposition," *J. Phys. Chem. C* **112**(43), 16784–16791 (2008).
34. A. J. Haes, W. P. Hall, L. Chang, W. L. Klein, and R. P. Van Duyne, "A localized surface plasmon resonance biosensor: First steps toward an assay for Alzheimer's disease," *Nano Lett.* **4**(6), 1029–1034 (2004).
35. T. Arai, P. K. R. Kumar, C. Rockstuhl, K. Awazu, and J. Tominaga, "An optical biosensor based on localized surface plasmon resonance of silver nanostructured films," *J. Opt. A, Pure Appl. Opt.* **9**(7), 699–703 (2007).
36. E. D. Palik, *Handbook of Optical Constants of Solids* (Academic Press, 1985).
37. S. L. Zhu, F. Li, C. L. Du, and Y. Q. Fu, "A localized surface plasmon resonance nanosensor based on rhombic Ag nanoparticle array," *Sens. Actuators B Chem.* **134**(1), 193–198 (2008).
38. B. Sepúlveda, P. C. Angelome, L. M. Lechuga, and L. M. Liz-Marzan, "LSPR-based nanobiosensors," *Nano Today* **4**(3), 244–251 (2009).
39. N. Menon, "Optical biosensors: applying photonics products to the biomedical diagnostics market," in *Optical Fiber Communication Conference (OFC)*, (Los Angeles, California, 2004).
40. G. P. Wiederrecht, *Handbook of Nanoscale Optics and Electronics* (Elsevier, 2010).
41. A. J. Haes and R. P. Van Duyne, "A nanoscale optical biosensor: sensitivity and selectivity of an approach based on the localized surface plasmon resonance spectroscopy of triangular silver nanoparticles," *J. Am. Chem. Soc.* **124**(35), 10596–10604 (2002).
42. S. M. Radke and E. C. Alcolija, "A high density microelectrode array biosensor for detection of E. coli O157:H7," *Biosens. Bioelectron.* **20**(8), 1662–1667 (2005).
43. C. Ruan, K. Zeng, O. K. Varghese, and C. A. Grimes, "Magnetoelastic immunosensors: amplified mass immunosorbent assay for detection of Escherichia coli O157:H7," *Anal. Chem.* **75**(23), 6494–6498 (2003).
44. A. Subramanian, J. Irudayaraj, and T. Ryan, "A mixed self-assembled monolayer-based surface plasmon immunosensor for detection of E. coli O157:H7," *Biosens. Bioelectron.* **21**(7), 998–1006 (2006).
45. S. L. Zhu, C. L. Du, and Y. Q. Fu, "Localized surface plasmon resonance-based hybrid Au-Ag nanoparticles for detection of Staphylococcus aureus enterotoxin B," *Opt. Mater.* **31**(11), 1608–1613 (2009).
46. S. L. Zhu, C. L. Du, and Y. Q. Fu, "Fabrication and characterization of rhombic silver nanoparticles for biosensing," *Opt. Mater.* **31**(6), 769–774 (2009).
47. C. D. Chen, S. F. Cheng, L. K. Chau, and C. R. C. Wang, "Sensing capability of the localized surface plasmon resonance of gold nanorods," *Biosens. Bioelectron.* **22**(6), 926–932 (2007).
48. M. M. Miller and A. A. Lazarides, "Sensitivity of metal nanoparticle surface plasmon resonance to the dielectric environment," *J. Phys. Chem. B* **109**(46), 21556–21565 (2005).

1. Introduction

The need for rapid, specific, sensitive, inexpensive, in-field and real-time detection of target analytes in solutions with an unknown content has made “biosensors” gain importance especially in fields such as environmental monitoring, pollutant detection, medical diagnostics, and biological warfare defense. A subcategory that biosensors are used is the detection of food-borne pathogens. Food borne pathogens cause infectious or toxic diseases upon the consumption of contaminated water and/or food. *Escherichia coli* (E.Coli O157:H7) is among the most serious food borne infections that also causes severe complications and sometimes fatal health problems, particularly among infants, children and the elderly.

There are several classical techniques to detect the presence of bacteria. Traditional methods like culture collection are effective but tests may take days to produce results and have limited ability in the discrimination of various bacterial strains [1]. There are newer, more rapid methods such as polymerase chain reaction (PCR) and Enzyme linked immunosorbent assay (ELISA) [2–4]. However, these methods require extensive pre-treatment prior to analysis, such as an enrichment step that involves growing bacteria on a nutrient agar to detectable levels; equipped laboratory and highly trained personnel who can operate the instruments and interpret the results.

These difficulties faced in classical detection methods have led to the development of different types of biosensors each relying on a different transduction mechanism. There are numerous optical [5, 6], amperometric [7, 8], impedometric [9], electro chemical [10], and magnetic [11, 12] biosensors described in the literature. These sensors are designed for tracking interactions at the classical physics limit, such as measuring mass, conductivity, pH, ionic mobility, and resonant RF frequency. However, optical sensors offer advantages such as immunity to electromagnetic interference, high sensitivity, and a fast response. They are capable of performing remote sensing and can provide multiplexed detection within a single device [13] and, therefore, are preferable.

When compared to other optical Propagating Surface Plasmon Resonance (PSPR) [6] or Surface Enhanced Raman Spectroscopy (SERS) [14–16] sensors, Localized Surface Plasmon Resonance (LSPR) systems are easy to manufacture and less expensive, in addition to being portable and practical. Working with small samples of analytes is possible and no special geometry (no specific angular conditions of excitation, no needs of prism coupler-based, grating coupler-based or optical waveguide) for detection is needed when compared with PSPR sensors.

PSPR and LSPR sensors both rely on detecting small changes in refractive index in the vicinity of a noble metal’s surface. Their sensitivities are caused by different mechanisms, but their overall sensitivities are approximately equivalent. PSPR sensors exhibit large refractive index sensitivities (2×10^6 nm RIU⁻¹) [17, 18]. The LSPR nano sensor, on the other hand, has modest refractive index sensitivity (2×10^2 nm RIU⁻¹) [18, 19]. However, the LSPR sensors’ enhanced sensitivity is due to the short and tunable characteristic electromagnetic field decay length that is on the order of 5-15 nm, whereas it is on the order of 200-300 nm for PSPR sensors [17, 18]. In addition, in PSPR systems, there is strong environmental temperature dependency due to the large refractive index sensitivity, whereas LSPR sensors do not require temperature control.

Moreover, PSPR sensors require at least a $10 \times 10 \mu\text{m}^2$ area for sensing. However, in LSPR sensing, confocal or near-field measurement techniques help minimize the area to a large number of individual sensing elements and even up to a single nanoparticle (NP). Finally, a UV-visible spectrometer is sufficient to obtain the extinction spectra, so that no complex equipment is necessary [20].

LSPR is based on the electromagnetic-field enhancement of metallic NPs. Periodic arrays of metallic nanostructures have been used for various applications such as plasmonic nano antenna arrays [21, 22]. The transmission and/or reflection spectrum obtained by illuminating the NPs with light, displays a resonance behavior located at an LSPR wavelength that is related with the NPs’ size, size distribution, and shape as well as the type of the metal used

and the surrounding environment [23]. LSPR biosensors work on the principle of detecting the refractive index changes of the environment that are induced by the presence of a chemical binding event occurring at the nano-patterned surface and measurement of LSPR wavelength shifts caused by this change [24–26].

LSPR is highly dependent on the size, shape, and period of the nanoparticles as well as the uniformity of the resultant structure. Chemical patterning methods such as Nano sphere lithography (NSL) are usually inexpensive and parallel-natured processes with high throughput. However, only limited shapes and arrays with hexagonal symmetry are feasible. Post deposition steps like thermal annealing or multi angle deposition are necessary for modification in shapes of nanostructures. Moreover, uniform areas are difficult to obtain [27].

EBL, on the other hand, is a modified SEM system that has superior properties compared to other optical or chemical patterning techniques, such as the precise placement and design of arbitrarily shaped NPs with a large selection of geometries of various sizes with fine features. It offers a high resolution of around 10 nm since it is not limited by diffraction limits unlike other optical lithography methods [28, 29]. Therefore, although advanced precision results in a higher cost and greater time, EBL serves academic research and development purposes the best [30, 31].

In this study, the size and period dependency of the LSPR wavelength and the way it can be tuned was shown through simulations and justified by reflection measurements. Surface functionalization was done for a biotin-avidin pair and verified by transmission measurements. The concentration dependency of the LSPR shifts was observed by changing the analyte concentrations. Real time binding measurements and refractive index sensitivity calculations were made. Finally, the sensor structure was applied and verified to detect *E. coli* bacteria.

2. Materials and methods

2.1 Chemicals

For this study, Polymethylmethacrylate (PMMA 950 A-2) was used as resist in e-beam lithography. EZ_Link Sulfo-NHS-SS-Biotin (21331) and Avidin (21121) were purchased from Pierce. 11-Amino-1-undecanethiol, hydrochloride [A423-10], and 6-Hydroxy-1-Hexanethiol were purchased from Probiol. *E. coli* O157:H7 Positive Control was purchased from KPL. The package includes heat-killed *Escherichia coli* O157:H7 cells, at least 3×10^9 cfu/mL in dextran solution. It is diluted in a 1/100 ratio, after being rehydrated with 1 mL of reagent quality water. Biotin labeled affinity purified antibody to *E. Coli* O157:H7 was also purchased from KPL. It is also received in lyophilized pellet form and diluted to 0.5 ug/ml after rehydration with 1 ml of reagent quality water.

2.2 Fabrications

Nanoparticle fabrication starts with the preparation of the sapphire substrate by spin coating PMMA 950 A-2, firstly at 500 rpm for 3 seconds and then at 4000 rpm for 40 seconds. The sample is then prebaked for 90 seconds on a hot plate heated to 180°C in order to evaporate the solvent in the photo resist and end up with a harder coating. A final step of aqua-save (polymer) coating at 4000 rpm for 40 seconds completes the preparation for EBL. After lithography with the “RAITH E-Line” system, the aqua-save is cleaned with DI water and then the sample is developed at an AZ 400K developer 1:4 for 30 seconds. After the development, the sample is cleaned in iso-propanol and blow-dried with nitrogen. The next step is the e-beam evaporation where an Ag coating of 30 nm is carried out in the “Leybold Univex 350 Coating System”. After evaporation, the samples are kept in acetone for lift off for 5-10 minutes, and then the excess metal is lifted off with an acetone flush onto the sample with a sterile glass injector. The final samples can be seen in Fig. 1(a), 1(b). The uniformity of the resultant samples can be seen from the histograms in Fig. 1(c), 1(d). The basic geometry allows for systematic tuning to the desired working wavelengths simply by changing the

diameters and deposited metal thickness during fabrication as well as enabling simulations highly correlated with fabrications, which saves labor during the optimization of sizes.

2.3. Surface functionalization

High affinity chemical pairs are used to test the validity of a biosensor before trials with real antigens and antibodies start. The avidin and biotin (Vitamin H) pair is the most extensively studied in bio-sensing applications, which is known for one of the strongest non-covalent interactions and their extraordinary affinity towards each other ($K_a = 10^{15} \text{M}^{-1}$). Biotin is a 244 Da vitamin found in small amounts in all living cells and avidin is a tetrameric protein that is usually found in egg whites [32]. In the current context, the surface functionalization refers to the steps taken for the immobilization of biotin on the Ag nano-disks and, therefore, to be ready to bind with (detect) the avidin in the target analyte. The same procedure is then applied to immobilize biotin labeled antibody and to sense the heat killed *E. coli* bacteria. Antibody and antigen pairs also have a high affinity towards each other. The use of affinity purified antibody ensures the high specificity for the target antigen and prevents cross-reactivity since they have lower backgrounds and lower nonspecific binding.

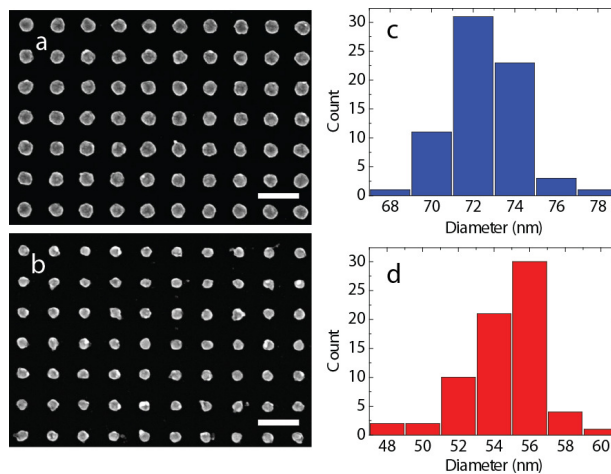


Fig. 1. EBL designed nano-disks. Period 150 nm; EHT is set as 10kV. (a) Diameter of nano-disks is about 73.21 nm, (b) Diameter of nano-disks is approx. 57.76 nm.

The surface functionalization starts by forming a self-assembled alkanethiol monolayer (SAM) on the surface of Ag nano-disks. This is not only necessary for binding biotin to the surface in a well ordered way but also a SAM layer is effective in avoiding the oxidation of Ag nanoparticles in aqueous solutions [33]. This is achieved by mixing 1 mM 11-amino-1-undecanethiol (11-AUT, Dojindo) and 1 mM 6-hydroxy-1-hexanethiol (6-HHT, Dojindo) 2-propanol solutions at a ratio of 1:3 for one hour. Using 6-HHT with 11-AUT reduces the non-specific adsorption and, therefore, increases the stability in the sensor response [34]. To remove nonspecifically adsorbed molecules after the incubation, the samples were rinsed with deionized water and dried with an N_2 blow after the incubation. Then, for bio-tinylation, 1 mM EZ_Link Sulfo-NHS-SS-Biotin (Pierce, 21331) was covalently linked to 11-AUT for at least three hours. Rinsing with DI water and N_2 blow-drying were repeated [35]. The samples with immobilized biotin were subjected to different concentrations of avidin (Pierce, 21121) solutions, and real time measurements were performed after rinsing and drying.

For the immobilization of biotin labeled affinity purified antibody to *E. coli* O157:H7, an SAM layer was formed following the same steps as described herein and then the samples were incubated in 0.5 ug/ml of antibody solution for at least 1 hour. *E. coli* O157:H7 Positive Control was prepared as described in the materials section and applied to the sensor surface.

2.4. Simulations

The simulations are done to computationally aid the design of nanostructures that give sharp and intense resonances that are necessary for sensitive detection, in turn avoiding the labor of fabrication and optical measurements.

The commercial software package “Lumerical”, which relies on “Finite-Difference Time-Domain Method” has been used in the simulations. The material data of sapphire and silver were taken from the literature [36]. The mesh sizes were set to values less than or equal to $\lambda/14$, where λ is the source wavelength divided by the refractive index of material of interest. The boundary conditions were set as perfectly matched layer (PML) in the direction of illumination for eliminating the undesired reflections from boundaries and periodic in the perpendicular plane for simulating a single unit cell and thereby saving simulation time. Numerical stability is ensured by setting the time step less than 0.02 fs based on the chosen mesh sizes.

Two sets of simulations were carried out to see the effect of changes in the period and diameter of nano-disks. In the first set of simulations, radii and the heights are held constant at 30 nm, and the period was varied 150-300 nm. The increase of the period without a change in radius, leads to a decrease in the density of the nanostructures and thereby a decrease in resonance intensity. See Fig. 2(a). In the second set of simulations, the period was held constant at 150 nm, height at 30 nm, and the diameter was varied between 30 and 73 nm. The increase in radius resulted in a red shift in the resonance wavelength and an increase in the intensity of the resonance wavelength. See Fig. 2(b).

Simulation results and reflection measurements are in good accordance, which can be seen from a direct comparison of Fig. 2(b) and 2(c). Any discrepancy may be attributed to the differences in the material data and physical dimensions used at the simulations and the fabricated design.

2.5. Measurements

In the present study, a reflection and transmission set-up has been prepared separately for the measurements using the same “Ocean-Optics” spectrometer, personal computer (PC), and a xenon light source (400-700 nm).

In reflection measurements, light from the Xenon source was transmitted to an Olympus microscope with a moving stage and camera, through an optical fiber ended with a collimator, and focused onto the sample using the collimating lenses of the microscope. The light was reflected from the sample and collected back with an optical fiber.

In transmission measurements light is transmitted by a multimode optical fiber to a 10x collimating lens that collects the light at the input and then to a 40x lens that illuminates the biosensor. The light is transmitted through the biosensor sample and collected by a 20x focus lens and then a 10 x collimating lens attached to the multimode fiber.

The collected light in both measurements are fed into the monochromator that diffracts it into its different frequency components. The photomultiplier of the monochromator that measures the intensity of each component is connected to the PC and the reflectance/transmittance data is saved using special software.

Three measurements are taken to obtain the respective spectrum: one to measure the total reflected/transmitted light, second to measure the background error due to losses in the optical path and the third to obtain the reflected/transmitted light from the nano-disk arrays. The reflectance/transmittance is the ratio of the sample light intensity to reference light intensity, where background noise is subtracted from both measurements separately. Similar measurement schemes are available from the literature [25, 26, 37].

Graphs showing the reflection with respect to the wavelength can be seen from Fig. 2(c). And the transmission measurements taken from the bio samples at every step of the surface functionalization are shown in Fig. 3.

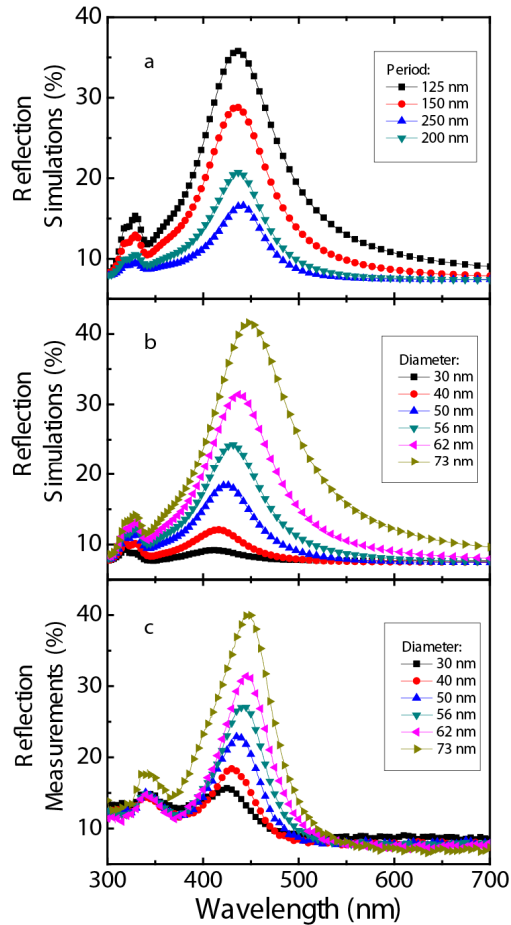


Fig. 2. (a) Reflection simulations: Radii and the height are held constant at 30 nm, and periods vary 150-300 nm. (b) Reflection simulations: Periods held constant at 150 nm, height is 30 nm, and the diameter varies 30-73 nm. (c) Reflection measurements: Periods held constant at 150 nm, height is 30 nm, and the diameter varies 30-73 nm.

3. Results and discussion

In this study, silver nano-disks on sapphire substrate are used as a sensor platform. Silver is selected since it has sharper and more intense LSPR than gold [38]. The chemical instability and oxidation issue of silver is overcome by designing a vacuum box to keep the samples in between measurements and fabrication steps. Sapphire is transparent at optical frequencies which makes it suitable for reflection and transmission measurements. And the dimensions are selected to keep the operation at around 400-500 nm. By this way it is guaranteed to stay at optical frequencies after surface modification steps that cause red shift. This will gain more importance in future studies that involve the detection of real pathogenic bacteria where more complicated surface functionalization may be necessary since working at this portion of the spectrum provides a means for gentle detection that does not destroy the structure of matter [39].

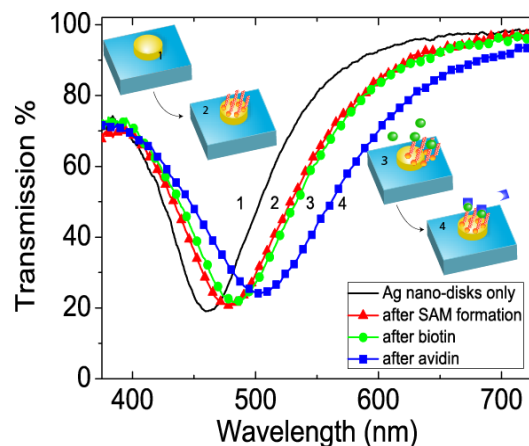


Fig. 3. Transmission measurement for silver NPs before application of chemicals (1), after the application of chemicals (2), after the application of biotin (3), and after the application of avidin (4). Inset: the schematic illustration of surface functionalization steps.

The first set of simulations and reflection measurements are in good correlation as can be seen in Fig. 2. In both, the increase in radius resulted in a red shift in the resonance wavelength and an increase in intensity of the resonance. Mie theory may help explaining these results. Although Mie theory is originally developed for describing the scattering properties of spherical nanoparticles, it is frequently used in getting an intuition about LSPR shifts in other geometries, too [40]. In Mie Theory, extinction (sum of absorption and scattering) is directly proportional with the density and cube of radius of the nanostructures. (See Eq. (1) below).

$$E(\lambda) = \frac{24\pi N_A r^3 \epsilon_m^{3/2}}{\lambda \cdot \ln(10)} \left[\frac{\epsilon_i(\lambda)}{(\epsilon_r(\lambda) + 2\epsilon_m)^2 + \epsilon_r^2(\lambda)} \right] \quad (1)$$

Here, λ is the radiation wavelength and $E(\lambda)$ is the extinction. N_A is the areal density and “ r ” is the radius of the nanoparticles. ϵ_m is the dielectric constant of the medium surrounding the metallic nanoparticles. ϵ_i is the imaginary portion and ϵ_r is the real portion of the metallic nanoparticles’ dielectric function.

When Mie theory is correlated with our first case (Fig. 2(a)) the increase of the period without a change in radius leads to a decrease in the density of the nanostructures. According to Mie Theory, this should lead to a decrease in reflection intensity, which is the case in the simulations where increasing the period led to a decrease in the amplitude of intensity.

In the second case (Fig. 2(b)), the increase in radius keeping the period constant is expected to increase the areal density of nanoparticles as well as the amplitude of resonance intensity that is fulfilled in both the simulations and measurements (Fig. 2(b), 2(c)). The wavelength dependency of the extinction on the dielectric constants of the medium and nanoparticles is also obvious from the equation. Since the equation is derived for spherical geometry, the dependence of LSPR shifts on the shape and the height is not very explicit.

Transmission measurements were performed after every step of surface functionalization to verify their success. Figure 3 depicts the LSPR wavelength shifts for the Ag nano-disks of the period 150 nm, height 30 nm, and diameter 60 nm. After the formation of SAM, the application of biotin and avidin; 15.9nm, 7.6 nm, 19.55 nm red-shifts were observed, respectively. These amounts of shifts are reasonable and sufficient to show that the binding events take place and the sensor has detected the applied material without any uncertainty.

An important feature of biosensors is their ability to determine the concentration of the analyte to be detected. Experiments have been conducted to verify that the designed sensor has different responses at different analyte concentrations and the measurements taken showed that the sensor has an adequate response at the 1nM-100nM range, which can be fitted

to a sigmoidal curve as shown in Fig. 4. Sigmoidal curves are used for describing the specific binding of bio-molecules due to the nature of binding [20, 34, 35, 41]. As the concentration of the analyte increases, the surface-receptors, namely biotin bound to the SAM formation on Ag nano-disks, start to saturate. The sigmoidal fit justifies the saturation as well as the steric hindrance effects that are expected as the concentration of the analyte increases.

Another experiment was conducted to see the real time binding, after the application of avidin. The measurements showed that the greatest response was observed shortly after the application of avidin within the first few minutes and the response was well saturated within half an hour. This experiment showed that the designed LSPR sensor has a fast response enabling real time detection, which is a very important feature for biosensors where the need of detection is urgent. The real time binding measurement results are provided in the inset of Fig. 4.

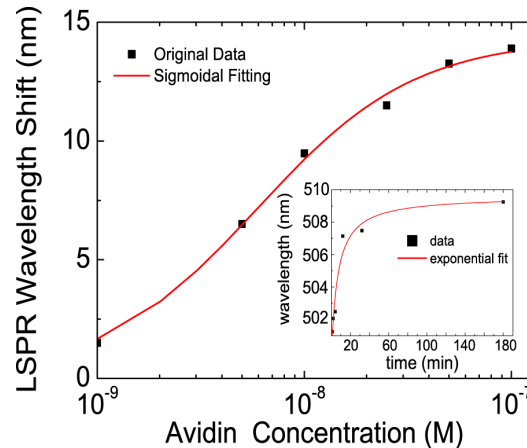


Fig. 4. LSPR wavelength shifts with respect to avidin concentration. A sigmoidal dependence was observed and fit by hill function (red curve; inflection point slope ~ -0.99). Inset: Real time binding, LSPR wavelength versus time after the application of avidin is shown. Real time measurements after 1 minute, 2, 4, 12, 32 minutes and 3 hours are taken.

After the verification of the sensor structure with a biotin-avidin pair, another trial with heat-killed *E. coli* was conducted. Since active *E. coli* bacteria can only be studied in BL2 (biosafety level 2) laboratories [42], heat-killed, potentially harmless positive controls were used in order to test the sensor structure [43]. The samples with immobilized antibody were subjected to a heat killed *E. coli* bacteria solution, and the transmission measurements were performed after rinsing and drying. To check for the repeatability of the results, a second measurement was taken after a second incubation of the sensor with the same bacteria solution. The results show that there is a red-shift of 4.5 nm after the application of bacteria and this measurement is stable and repeatable (Fig. 5). For the time being, this trial only shows the possibility of such a sensing method. Specificity and concentration dependency should be studied before calling the sensor an *E. coli* sensor. A limit of detection study is not done yet. However, our current *E. coli* detection concentration of $\sim 10^7$ cfu/ml is comparable to the direct assay detection limit of 10^6 cfu/ml for a surface plasmon immunosensor for the detection of *E. coli* although it is much smaller than the sandwich assay detection limit of 10^3 cfu/ml for the same sensor [44]. It should be noted that no optimization studies have been performed yet, so there is still room for improvement.

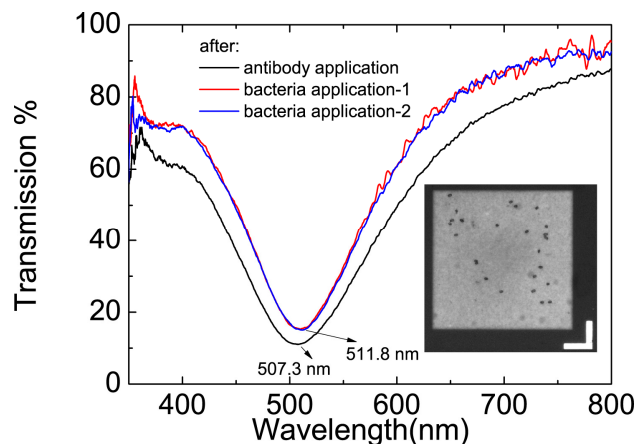


Fig. 5. Transmission measurements after incubation in antibody and *E. coli* positive control solutions inset: Dark-field Electron-microscope image of the sensor surface after the bacteria is applied. The applied bacteria look like cylindrical rods. The square shaped sensor area is 50 μ m x 50 μ m.

An important feature of biosensors is refractive index sensitivity, which can be defined as the response of the resonance peak wavelength to changes in the bulk refractive index of the surrounding environment. In this study, we obtained the refractive index sensitivity through calculations based on transmission measurements. The sensors are exposed to iso-propanol ($n = 1.3776$) and water ($n = 1.3325$) and transmission measurements were taken while the samples were incubated in the solutions. The refractive index sensitivity was then calculated using the peak resonance wavelengths obtained through the transmission measurements using the formula $\Delta\lambda/\Delta n$; where Δn is the change in the refractive index of the dielectric environment and $\Delta\lambda$ is the experimentally measured shift in the peak resonance wavelength. A refractive index sensitivity value of 221 nm/RIU was obtained for 40 nm diameter silver nano-disks and 354 nm/RIU for 80 nm nano-disks both with period 150 nm. These values are comparable to those obtained in the literature for different types of LSPR sensors that range between 191 and 366 nm/RIU [19, 37, 45–48].

Another important comparative parameter of sensing devices is the figure of merit $FOM = (\Delta\lambda/\Delta n) \cdot (1/\Delta w)$, where Δw is the FWHM (full-width at half-maximum) of the resonant dip. This parameter figures out the ability of the sensor to accurately measure small changes in the resonance wavelength considering the sharpness of the resonance behavior. Although there is an improvement in the sensitivity factor with the increase in diameter, FOMs calculated for the two cases described above are close to each other: 2.33 and 2.81 since the FWHM increases from 95 nm to 126 nm as the diameter increases. In the experimental trials we have chosen 60 nm diameter nanoparticles for their good sensitivity and moderate FWHM values considering the above calculations.

4. Conclusions

In this study, EBL designed silver nano-disks are shown to be used as label free nano-biosensors based on LSPR and verification is done through simulations and optical measurements.

Simulations are important since they can avoid unnecessary fabrications especially when the structure has to be tuned to a desired wavelength. In many other methodologies, LSPR substrates are hardly repeatable and the resultant sizes are not predictable so that the structure has to be fabricated to gain an intuition about the resonance frequency [33, 35].

It is possible to extend the detection of heat killed *E. coli* bacteria for the detection of other pathogenic bacteria since biotin is capable of being conjugated to many proteins without altering their biological activity. If biotin conjugated antibody of specific bacteria is

immobilized onto the sensor then similar steps can be taken to detect the presence of its antigen in target solution. By this method, one can even achieve multi-output sensor chips that can detect several types of bacteria simultaneously.

Future study includes examining the concentration dependency, specificity, reversibility, selectivity, and optimization of the sensor. The detection of bacteria in solutions, food, and biological and medical samples and the design of a handheld, portable device comprising its own light source, spectrometer, and sample holder is the next step. The technique can then be used in the continuous monitoring of food and water supplies, to protect against terrorist attacks, or speed up the identification of the species when time is of essence for medical treatment.

Acknowledgments

This work is supported by the European Union under the projects PHOME, ECONAM, and N4E, and TUBITAK under the Project Nos. 109E301, 107A004, and 107A012, and DPT under the project DPT-HAMIT. One of the authors (E.O.) also acknowledges partial support from the Turkish Academy of Sciences.